

# Analysis of Dynamic Impatt Oscillations caused by Radiation Induced Deep Centers

Ralf Siemieniec<sup>\*</sup>, Josef Lutz<sup>\*\*</sup>, Reinhard Herzer<sup>\*\*\*</sup>

<sup>\*</sup>Technical University of Ilmenau, Department of Solid-State Electronics,  
PO BOX 100565, D-98684 Ilmenau, Germany, e-mail: ralf.siemieniec@tu-ilmenau.de

<sup>\*\*</sup>Technical University of Chemnitz, D-09107 Chemnitz, Germany

<sup>\*\*\*</sup>Semikron Elektronik GmbH, Sigmundstraße 200, D-90431 Nuernberg, Germany

**Abstract.** The occurrence of high-frequency impatt oscillations is related to the presence of charged deep donor-states as generated by irradiation processes for carrier-lifetime control. This effect is well-known in electron-radiated devices. Device simulation predicts a similar effect in locally lifetime-controlled helium-radiated devices. The experiment gives an approval of the simulation results but shows some unexpected effects too.

## INTRODUCTION

Dynamic impatt (impact ionization transit time) oscillations are high-frequency oscillations which occur in carrier-lifetime controlled silicon power devices in the low working temperature range (app.  $T < 280\text{K}$ ) at voltages well below the static breakdown voltage [1]. They are caused by temporarily positive charged deep donors  $\text{H}(195\text{K})$  – related to the carbon-vacancy complex  $\text{COVV}$  – which are induced by irradiation and annealing.

The avoidance of these high-frequency oscillations is necessary because of their adverse influence on the drive control units and because of EMC issues.

Similar effects of charged deep levels are also known from devices based on SiC materials [2].

## EXPERIMENTAL SETUP

Measurements are done using a conventional double-pulse method. All devices have a doping profile as shown in Fig. 1. After irradiation, all samples are annealed at  $T > 600\text{K}$  for 1h. Fig. 2 gives

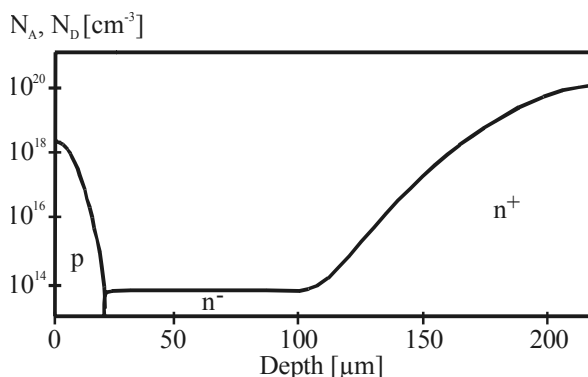


Fig. 1: Basic structure of 1200V / 150A/cm<sup>2</sup> diode

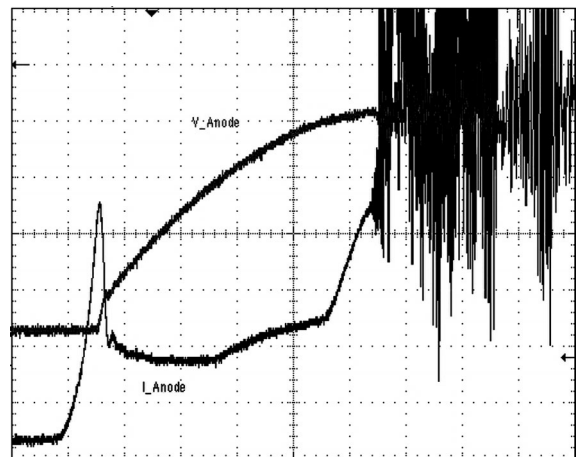


Fig. 2: Oscillogram of an impatt oscillation,  $T=275\text{K}$ ,  $V_R=790\text{V}$ ,  $J_F=15\text{A/cm}^2$  (5A/div, 200V/div, 200ns)

an example of a measured impatt oscillation of an electron-radiated diode ( $E=4.5\text{MeV}$ ,  $d=1\text{E}15\text{cm}^2$ ).

## SIMULATION MODEL

The dynamic impatt oscillation is simulated in 2D using an extended recombination model, shown in Fig. 3, considering the relevant number of recombination centers as well as their time-dependent charging processes [3]. The simulations are based on carefully determined recombination center data [4].

## INVESTIGATION OF ELECTRON-RADIATED SAMPLES

Fig. 4 shows a simulation of an impatt oscillation, using a simple series circuit of a time-variable resistor, a small inductance and an electron-radiated diode structure according to Fig. 1 ( $E=4.5\text{MeV}$ ,  $d=1\text{E}15\text{cm}^2$ ). During the turn-off, the generated donor-states are positively charged and increase the background doping, which usually sustains the blocking voltage. Avalanche breakdown occurs at the pn-junction region due to the high electric field, which is shown in Fig. 5 for several points in time, and generates electrons. These electrons counterbalance the positive donors and hence stop the avalanche generation of carriers.

Therefore, the avalanche generation rate changes

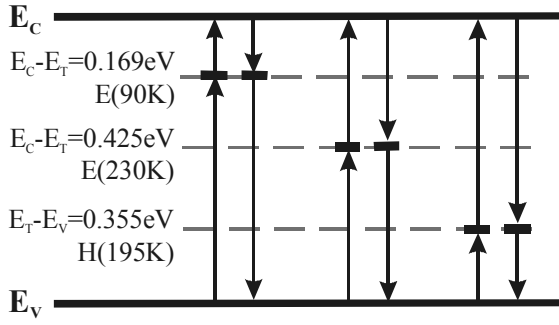


Fig. 3: Recombination model and centers as used for device simulation

with time. Due to the electric field, the electrons are transported to the  $nm^+$ -junction and again, avalanche generation starts at the  $pn$ -junction.

Fig. 6 shows the electron densities along the vertical axis for different points in time. The frequency of the oscillation is related to the transit-

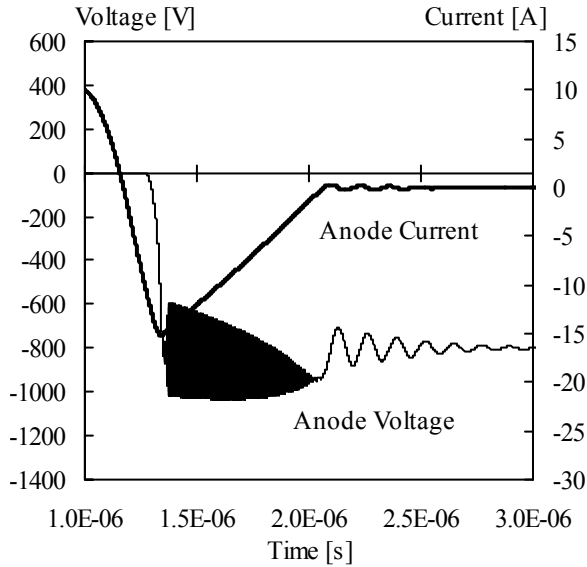


Fig. 4: Simulation of temporary impatt oscillation,  $T=300K$ ,  $V_R=800V$ ,  $J_F=15A/cm^2$

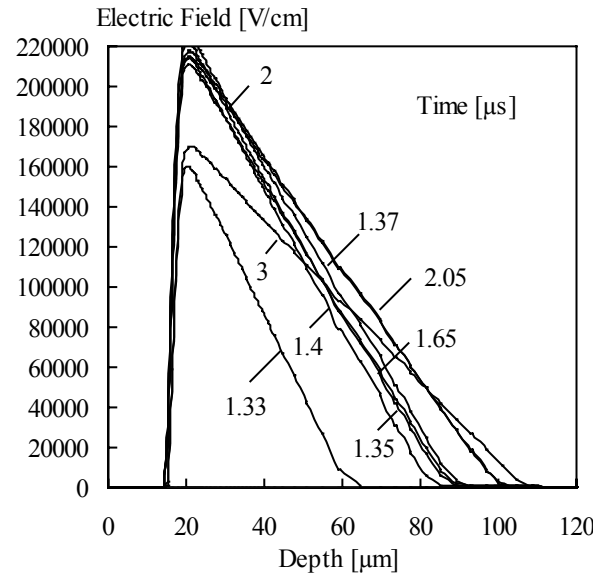


Fig. 5: Electric Field along vertical axis vs. time

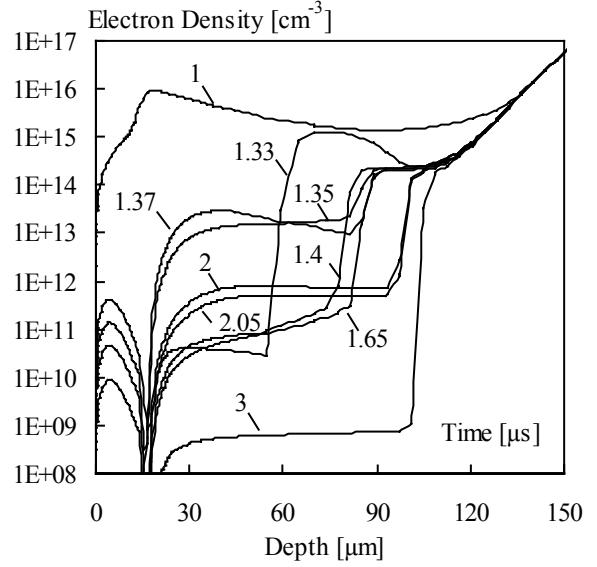


Fig. 6: Electron densities at different points in time

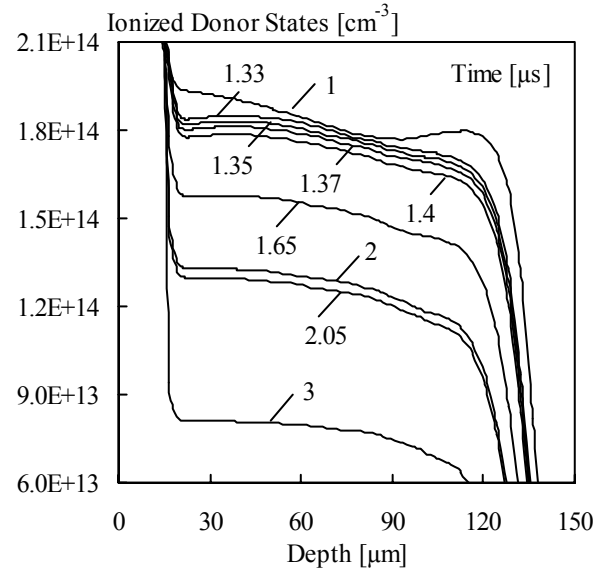


Fig. 7: Density of ionized donor-states vs. time

time which is needed by the electron flow through the low-doped region of the device, depending on the carrier saturation velocity  $v_d$  and the width of the low-doped region  $w_B$ :

$$f \approx \frac{v_d}{w_B} \quad (1)$$

The measured oscillation frequency for the electron-radiated device (see Fig. 2) is in the range of 850...950MHz in agreement with [1]. The determination of the frequency is difficult due to interfering noise and resolution capability.

The impatt oscillation stops as soon as the positive donors are discharged, according to the time constant which depends on the center concentration and the capture rates. The device is now able to withstand the reverse voltage [1]. Fig. 7 shows the reduction of density of the charged donor-states with time.

The onset of this effect depends mainly on the concentration of the deep donors and of the temperature. Fig. 8 shows the comparison of

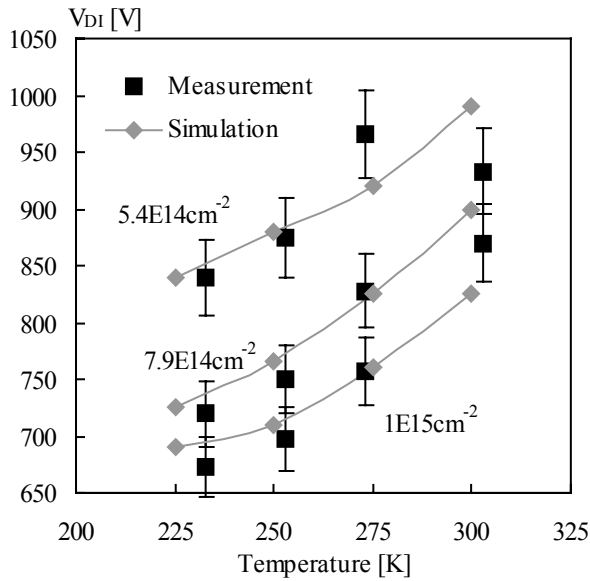


Fig. 8: Threshold voltage of impatt oscillation for 4.5MeV electron-radiated devices in dependence of temperature and irradiation dose. Measured values taken from [1]

measured and simulated values of the onset voltage of impatt oscillations on electron-radiated recovery diodes. The simulated and measured values show a sufficient accordance.

### INVESTIGATION OF HELIUM-RADIATED SAMPLES

**Preliminary Simulations.** For local recombination center profiles (as generated by use of helium ions) in the low-doped region of the device, device simulation predicts the occurrence of impatt oscillations. Fig. 9 gives the center profiles as used in the preliminary simulations. Fig. 10 shows, as an example, one result of the device simulations for a diode with a deep local recombination center profile.

**Experimental Results.** Helium irradiation with an energy of 11MeV was applied from the top side to samples with an active area of 0.1cm<sup>2</sup>. Two different

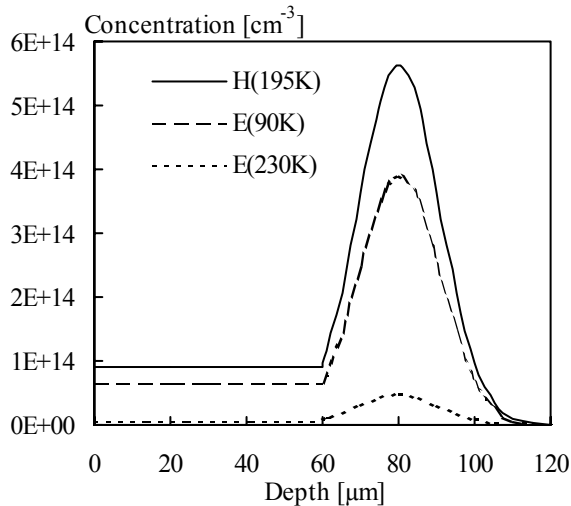


Fig. 9: Recombination center profile for simulation

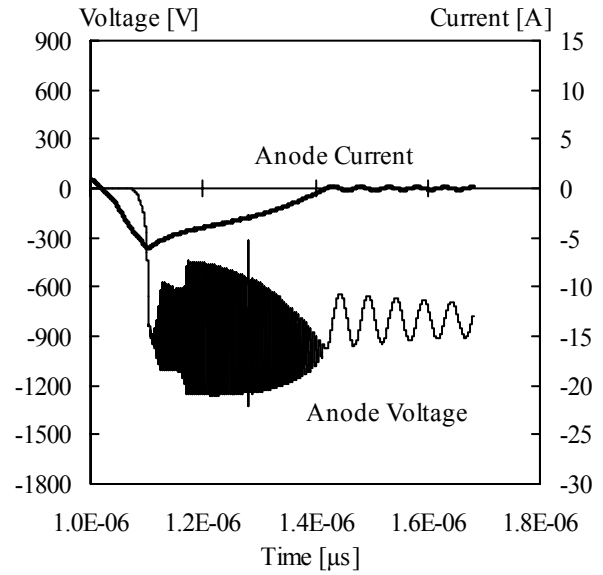


Fig. 10: Simulation of temporary impatt oscillation of a device with local recombination center distribution,  $T=300K$ ,  $V_R=800V$ ,  $J_F=15A/cm^2$

radiation doses of  $1.4 \cdot 10^{12} cm^{-2}$  and  $2.1 \cdot 10^{12} cm^{-2}$  are used (samples He14 and He21, respectively).

Fig. 11 shows a measurement of an impatt oscillation at the device He21. In difference to electron-radiated devices, additional two current peaks are to be seen before the oscillation starts. There is no sharp threshold voltage of the oscillation at the samples He21. The voltage amplitude of the oscillation is much lower for helium-radiated devices compared to electron-radiated devices. The oscillation frequency, app. 1.4...1.6GHz in the measurement of He21, is higher compared to the oscillation frequency of electron-radiated samples.

**Discussion.** A qualitative explanation for the different behavior of the helium-radiated devices is given by the simulation results of structures with a recombination center profile as shown in fig. 9. Fig. 12 shows the electric field at different points in time which is now trapezoidal as it were in presence of an additional n-doped buffer layer. This is caused by the

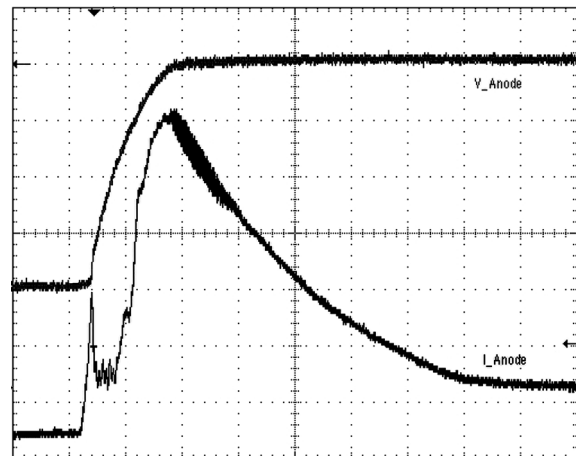


Fig. 11: Measurement of impatt oscillation at He21,  $T=275K$ ,  $V_R=790V$ ,  $J_F=15A/cm^2$  (2A/div, 200V/div, 200ns)

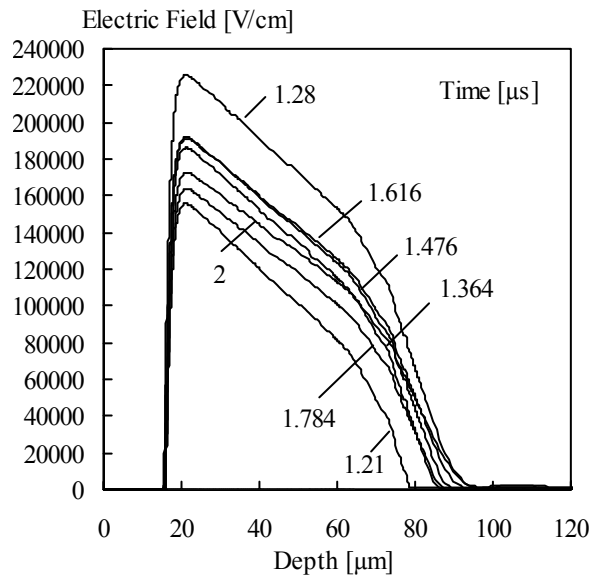


Fig. 12: Simulation of electric field along vertical axis vs. time for a helium-radiated diode structure

ionized donor-states, shown in Fig. 13, which obviously act as a kind of temporarily buffer layer. Thus, the width of the low-doped region is reduced and the oscillation frequency rises.

Now, in case of the helium-radiated samples, there is no definite threshold voltage. The oscillation starts almost inappreciable and is therefore difficult to measure due to the interfered noise. Consequently, the reverse voltage is measured at a condition, where the avalanche-related current peak reaches a previously assigned value. Fig. 14 shows the temperature dependent voltage for an avalanche current density of  $30\text{A}/\text{cm}^2$ . Now, the temperature dependency is  $1.1\text{V}/\text{K}$  compared to  $2.2\text{V}/\text{K}$  in case of electron-radiated devices. The changed shape of the electric field, trapezoidal instead of triangular, results in a weaker temperature dependency of the avalanche generation. This is in coincidence with a rough analytical estimation, based on an abrupt junction and

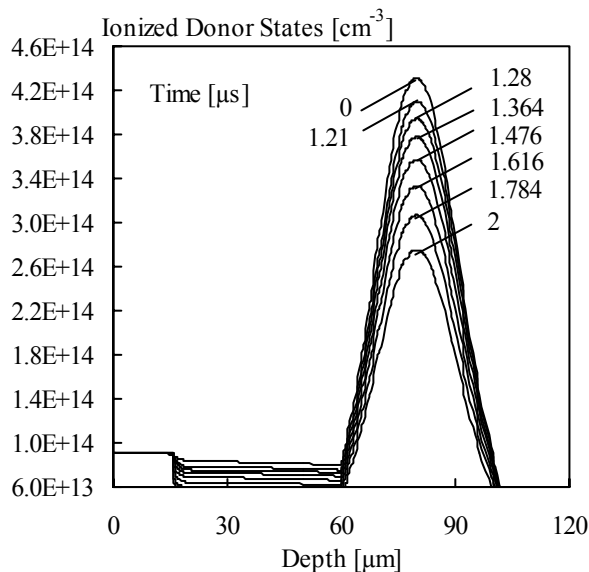


Fig. 13: Density of ionized donor-states vs. time in a simulated helium-radiated diode structure

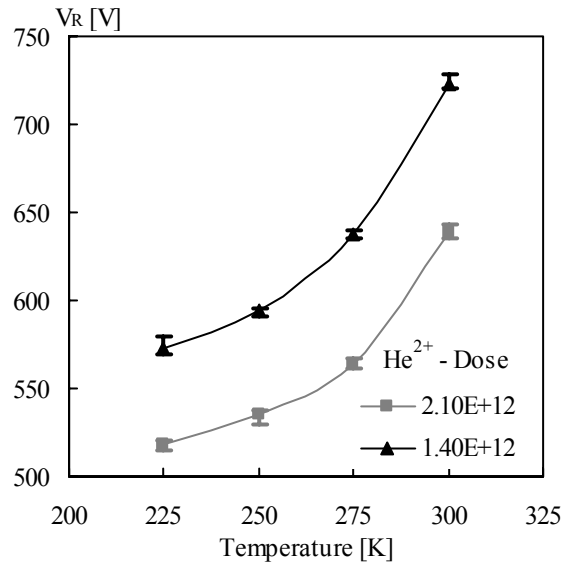


Fig. 14: Temperature dependence of reverse voltage for an avalanche current of  $30\text{A}/\text{cm}^2$  (helium-radiated samples)

the ionization coefficients in [5] with the temperature dependency given in [6].

## CONCLUSION

Transit-time oscillations created by temporarily charged deep levels are found in electron-radiated devices as well as in high-energy helium-radiated devices. The specific behavior of the helium-radiated devices is explained by the formation of a temporarily n-buffer due to the temporarily positively charged donor-states of generated centers. Further investigations are necessary to understand all effects in these devices.

## REFERENCES

- [1] Lutz, J., Südkamp, W. and Gerlach, W.: Impatt Oscillations in Fast Recovery Diodes due to Temporarily Charged Radiation-Induced Deep Levels, *Solid-State Electronics*, 42 (6), 1998, 931-938
- [2] Domeij, M., Breitholtz, B., Åberg, D., Martinez, A. and Bergman, P.: Dynamic Avalanche and Trapped Charge in 4H-SiC Diodes, *Proc. 8th Internat. Conf. on Silicon Carbide, III-Nitrides and Related Materials*, Materials Science Forum, 1327, 338-342, 2000
- [3] Siemieniec, R., Lutz, J.: Axial Lifetime Control by Radiation Induced Centers in Fast Recovery Diodes, *Proc. ISPS (Prague 2002)*, 83-90
- [4] Siemieniec, R., Südkamp, W. and Lutz, J.: Determination of Parameters of Radiation Induced Traps in Silicon, *Solid-State Electronics*, 46(6), 2002, 891-901
- [5] Fulop, W.: "Calculations of Avalanche Breakdown Voltages of Silicon pn-Junctions", *Solid-State Electronics*, 10, 1967, 39-42
- [6] Singh, R., Baliga, B.J.: "Analysis and optimization of power MOSFETs for cryogenic operation", *Solid-State Electronics*, 36(8), 1993, 1203-1211